Ore Geology Reviews 101 (2018) 468–480

Contents lists available at ScienceDirect

Ore Geology Reviews

journal homepage: www.elsevier.com/locate/oregeorev

Combined tectonic and paleogeographic controls on the genesis of bauxite in the Early Carboniferous to Permian Central Yangtze Island

Ruixue Wang[a,b], Qingfei Wang[a,*], Yuanxiao Huang[a], Shujuan Yang[a], Xuefei Liu[a], Qi Zhou[c]

[a] State Key Laboratory of Geological Processes and Mineral Resources, China University of Geosciences, Beijing 100083, PR China
[b] Commonwealth Scientific and Industrial Research Organization, Mineral Resources, ARRC, Kensington, Western Australia, Australia
[c] Guizhou Bureau of Geology and Mineral Exploration and Development, Guiyang 550004, PR China

ARTICLE INFO

Keywords:
Bauxite
Detrital zircons
Sediment provenance
Sedimentary facies
South China

ABSTRACT

Two bauxite horizons, with a total reserve of 1.29 Bt, occur in the Lower Carboniferous and Lower Permian in the central South China Block. Different from other intracontinental bauxites in China, which are genetically linked to the orogenesis along the continental margin, these bauxites were generated in the absence of marginal orogenesis. The genesis of these bauxites were studied based on tectonic, paleogeographic, and paleoclimatic controls. The orebody in Huofengchong (HFC) region is hosted within the Lower Carboniferous, which overlies upon the Cambrian dolomite unconformably. The orebody in the regions of Yanfengba (YFB) and Baiyantou (BYT) occurs in Lower Permian, which overlies upon the Silurian shale or Devonian dolomite unconformably. The mineral assemblages in the Carboniferous HFC bauxite consist of diaspore, illite, anatase, and in Permian YFB and BYT bauxite, the minerals are diaspore, anatase, illite, clinochlore, and kaolinite. The data from the U-Pb isotope measurements of detrital zircons from these bauxites provide two main ages: (1) a maximum U-Pb age peak of ca. 800 Ma from the Carboniferous HFC and (2) a maximum age peak of ca. 1100 Ma for the Permian BYT and YFB. The ca. 800 Ma detrital zircons from the Carboniferous bauxite are dominating in the Paleozoic sedimentary units, which likely derive from the erosion of the Mid- to Neo-proterozoic felsic volcanic and intrusive rocks (Panxi-Hannan arc) occurring in the western margin of the South China Block. By contrast, the zircons with ages of ca. 1100 Ma are prevalent in the Paleozoic sediments from the center of the block. The above results indicate that the Lower Carboniferous and Lower Permian bauxites are sourced from the sedimentary rocks in the western and central parts of the South China Block, respectively. Despite the difference in the provenance, these two episodes of deposits were both deposited in a tidal flat-restricted platform attached to an EW-trending Yangtze island, occupies the western to central parts of the South China block. This indicates that the shift from a marginal to central uplift within the paleo-island from Early Carboniferous to Early Permian has induced the transition in the provenance of the source material. In addition, the weathered materials from the two provenances both accumulated in the coastal region receiving further bauxitization. The bauxitization was boosted by the persistent preferable tepid and humid paleoclimate, defined by the equatorial position of South China block and the drop of global temperature during the metallogenic period.

1. Introduction

Bauxites are economic to sub-economic concentrations of aluminium and are commonly classified into two main categories: karstic bauxites overlying carbonate rocks and lateritic bauxites overlying aluminosilicate rocks (Bárdossy, 1982; D'Argenio and Mindszenty, 1995). Most lateritic bauxites, which derive from the *in situ* weathering of aluminosilicate-rich protolith, have textures and compositions comparable with their underlying rocks (Horbe and Costa, 1999; Mutakyahwa et al., 2003). In contrast, karstic bauxites are dominantly allochthonous (Bárdossy, 1982; Liu et al., 2012, 2017b; Yang et al., 2017; 2018). Understanding the genesis of karstic bauxite needs to consider several factors including provenance, paleoclimate, paleogeography, and regional tectonics, as well as exposure duration (Bárdossy, 1982; Bogatyrev et al., 2009). Karstic bauxites were suggested to have closer relationship with regional tectonics than the lateritic ones (Nakano et al., 2017; Wang et al., 2015; Yu et al., 2015; Cai et al. 2015; Deng et al., 2010). From the research on the bauxite located

* Corresponding author at: State Key Laboratory of Geological Processes and Mineral Resources, China University of Geosciences, Beijing No. 29 Xueyuan Road, Beijing 100083, PR China.
E-mail address: wqf@cugb.edu.cn (Q. Wang).

https://doi.org/10.1016/j.oregeorev.2018.07.013
Received 17 May 2018; Received in revised form 5 July 2018; Accepted 17 July 2018
Available online 19 July 2018
0169-1368/

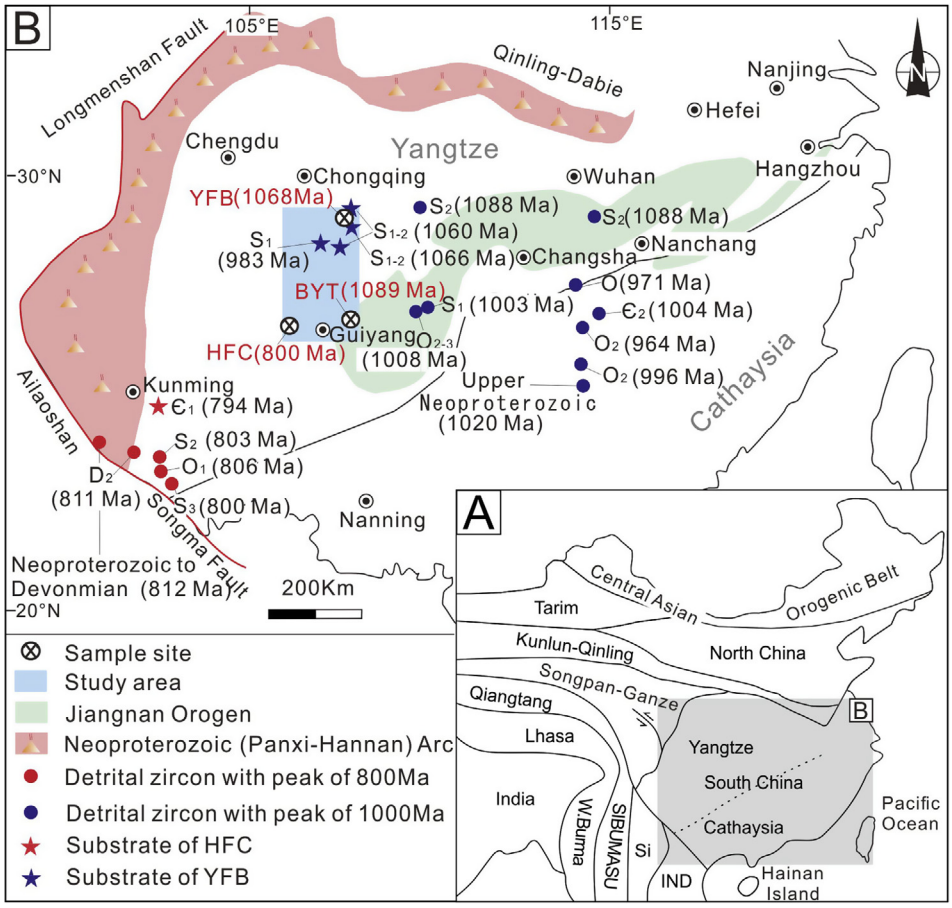

Fig. 1. (A) Simplified tectonic map of China. The rectangle highlights the position of the South China Block, displayed in Fig. 1B. (B) Enlargement of the South China Block, displaying the location of Neoproterozoic Panxi-Hannan arc and Jiangnan Orogen, and the prominent Precambrian peaks of detrital zircon ages in the Cambrian to Devonian sedimentary units (modified after Gu et al., 2013).

in the North China Craton (Wang et al. 2015; Cai et al., 2015), it was proposed that the orogenesis along the continent margin has triggered both the formation of continental basins and the erosion of the orogeny itself. In this framework, the sedimentation of the material deriving from the orogeny in the continental basins, together with the occurrence of the proper climatic conditions, resulted in bauxitization.

Two bauxites horizons formed in Early Carboniferous and Early Permian in the central South China Block. The accumulated reserves of the bauxite were 1.29 billion t by 2014 (Liu et al., 2016). The bauxites are mainly karstic type and are relatively concentrated in Guiyang, Zunyi, Huangping-Kaili and Wuchuang-Zhengan-Daozhen (WZD) area (Fig. 4). The average grade of these bauxite is 56.5–67.3%.

The South China Block had a passive margin during the bauxitization periods. This provides us a precious chance to explore the genesis of bauxite formed in an intracontinental setting without impact of simultaneous orogenesis in the marginal areas. The mineralogy and geochemistry of the bauxites along with the source materials have been investigated in previous studies (Ling et al., 2015, 2017; Long et al., 2017; Gu et al., 2011; Wang et al., 2013; Li et al., 2013). However, the controls on the episodic production of bauxite in the intracontinental setting were barely discussed. This study presents new mineralogical and geochronological data for bauxite ore, ferric clay, and aluminous clay and detrital zircons associated with bauxite deposits of the central South China Block. These data are combined with paleoclimatic and paleogeographic investigations to restore the metallogenic conditions for these intracontinental bauxites and complete the knowledge of the bauxite genesis.

2. Regional geology

The South China Block is separated from the North China Craton to the north by the Qinling-Dabie orogen, from the Songpan-Ganze terrane to the northwest by the Longmenshan Fault, and from the Indochina Block to the west by the Ailaoshan-Songma suture zone (Zhao and Cawood, 2012; Deng et al., 2017) (Zhao and Cawood, 2012). The South China Block is bounded to the east by the Pacific Ocean, which has initiated the subduction until Late Permian (Fig. 1A) (Liu et al., 2017). The Ailaoshan-Songma suture formed by the closure of the Paleo-Tethys Ailaoshan Ocean as a result of westwards subduction (Yang, 2018; Wang et al., 2014). The Ailaoshan Ocean initially opened as a back-arc basin along the northern margin of Gondwana during the Late Cambrian to Early Devonian. Then it developed into a mature ocean basin in Late Devonian to Early Carboniferous. Finally, it became a remnant oceanic basin and closed in late Permian to Early Triassic via the west-dipping subduction (Metcalfe, 2006; Jian et al., 2009). It was shown that from the Early Carboniferous to the Middle Permian, the South China Block has not witnessed oceanic subduction along its margins.

The South China Block is divided into the Yangtze Block in the northwestern part and the Cathaysia Block in the southeastern part separated by the Jiangnan Orogen (Fig. 1B) (Cawood et al., 2013; 2017;

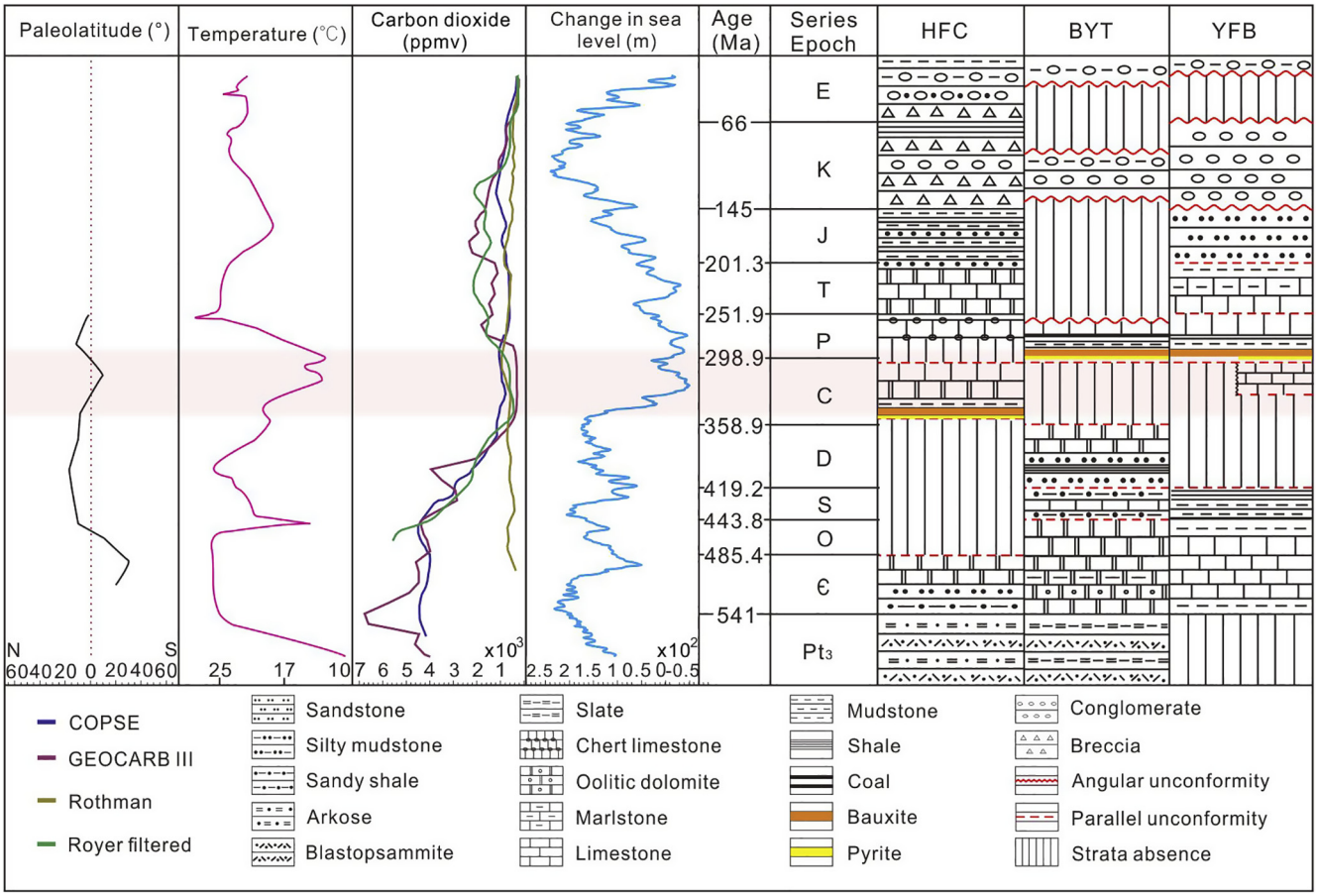

Fig. 2. Stratigraphic columns of the study area and logs representing the paleolatitude of South China Block (Cocks and Torsvik, 2013), temperature changing trend (Came et al., 2007), atmospheric carbon dioxide (Berner, 1990), sea-level change (Ross and Ross, 1988). COPSE: measurements of CO_2 were made by application of a soil carbonate CO_2 paleobarometer to a suite of paleosols that share key physical and chemical characteristics; GEOCARB III: models the carbon cycle on long time scales. The long-term carbon cycle is primarily geochemical, a result of the exchange of carbon between the atmosphere and rocks. Rothman: based on considerations related to the chemical weathering of rocks, volcanic and metamorphic degassing, and the burial of organic carbon, along with considerations related to the stable isotopic composition of organic carbon and strontium in marine sedimentary rocks. Royer filtered: based on $\delta^{18}O$ measurements and factoring in seawater pH levels. A 30 myr average filter is applied to the data.

Zhao et al., 2011; Li et al., 2009). The Jiangnan Orogen is made up by an Archean-Paleoproterozoic crystalline basement surrounded by Late Mesoproterozoic to Early Neoproterozoic folded belts. The occurrence of ~1000 Ma igneous rocks suggests a tectono-thermal event, which is well represented in throughout the Jiangnan Orogen (Zhao, 2015). The bauxite cluster region is located northwest on the Jiangnan Orogen. Along the western and northern margins of the block is the Panxi-Hannan belt (Fig. 1B). The belt was generally considered as a continental margin arc that lasted at least from 860 Ma to 800 Ma, deduced from the geochemistry of Neoproterozoic *meta*-volcanics and coeval plutons (Zhao and Cawood, 2012). The basement rocks of the central South China Block are unconformably overlain by Neoproterozoic to Lower Paleozoic sediments, which are separated by a paraconformity from Devonian siliciclastic sediments and Carboniferous or Permian limestone successions. The lower Paleozoic successions consist of carbonate and siliciclastic successions. The Cambrian unit consists of sandstone and limestone. The Ordovician succession is composed of limestone with minor dolomite and mudstone. Moreover, Lower Silurian strata are dominated by shale and sandstone (Fig. 2) (Wang et al., 2010).

During Late Cambrian, a continental setting was present in the western margin of the South China Block, gradually passing into tidal flat facies and restricted platform, open platforms, and deep sea (Fig. 3A). Then in the Ordovician, most of the southern South China Block became exposed. Later in Silurian, the northern part of southern South China Block was covered by platform, tidal flat facies and restricted platform (Fig. 3B). During the Devonian the paleogeographic setting was significantly altered as a continental mass appeared in the central part, which joined the western uplift and formed an EW-trending strip of land (Fig. 3C). This land was an independent island in the Paleo-Tethys Ocean, and is called “Central Yangtze Island” in the present study since it is mainly located at the Yangtze Block. The Central Yangtze Island was surrounded by tidal flat facies and restricted platform along its southern and northern margins and lasted throughout the Late Carboniferous though its spatial range varied to a small extent. In the Early Carboniferous to Permian, bauxite developed on the northern and southern margin of the Yangtze island (Fig. 3D).

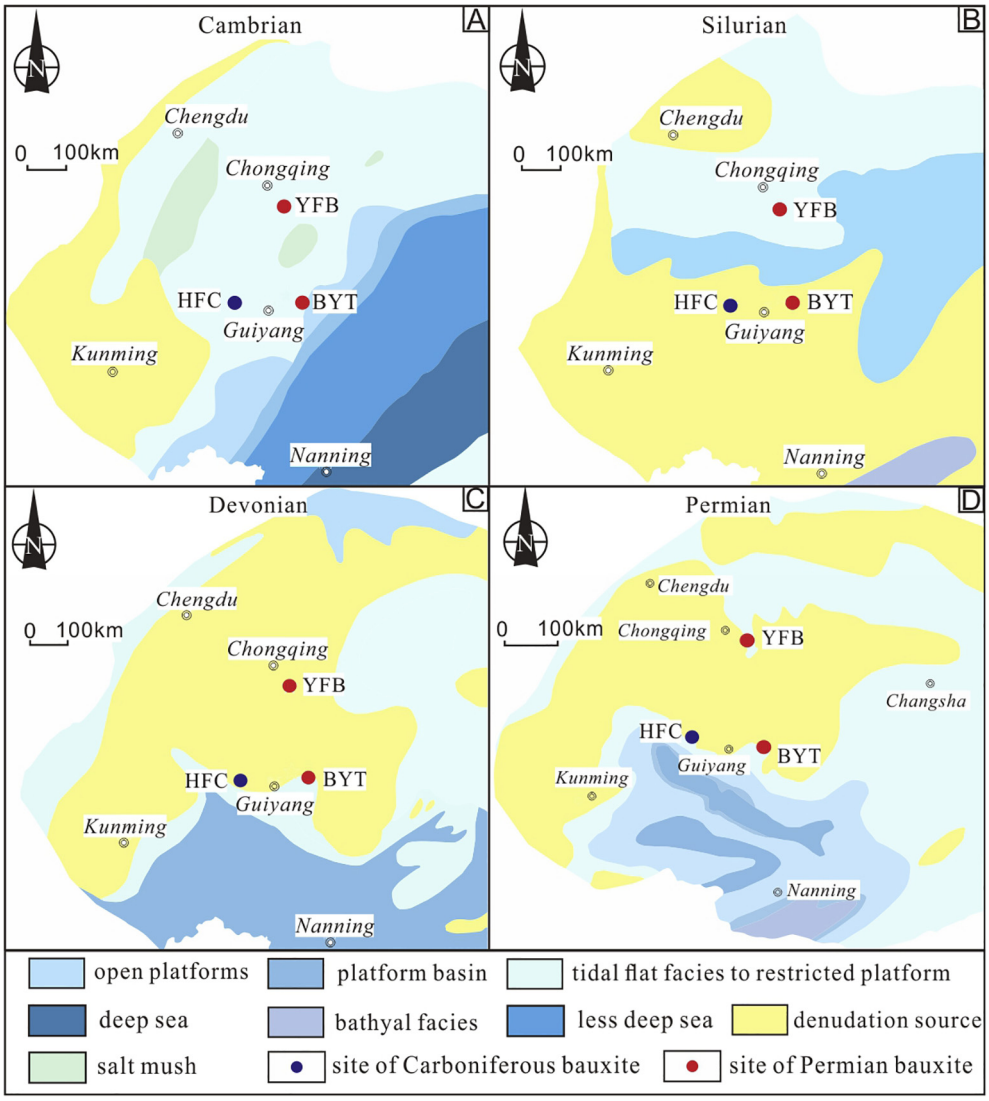

Fig. 3. Paleogeography of the South China Block from Late Cambrian to Early Permian. (A) Late Cambrian; (B) Early Silurian; (C) Late Devonian; (D) Early Permian. Revised from Ma et al. (2009) and Cui (2014).

3. Deposit geology

For the present study three bauxite deposits were selected: the Huofengchong (HFC) bauxite (N 26°33.330′, E 106°15.168′) is located northwest of Guiyang City, Baiyantou (BYT) bauxite (N 26°43.097′, E 107°46.343′) is located between Huangping and Kaili County, and the Yanfengba (YFB) bauxite (N 29°05.019′, E 107°41.586′) occurs nearby the northern Daozhen County (Fig. 4).

Phanerozoic rocksare well exposed in the HFC area. The Precambrian lithologies are mainly blastopsammite and arkose. Cambrian sediments are composed of sandstone, claystone, microcrystalline dolomite and yellow–green clay rocks. Lower Carboniferous strata contain dolomite, mudrocks transitional to bauxite-rich clay units and bauxite orebodies. Permian quartz sandstone and thick limestone with chert covered the Carboniferous unit (Figs. 2 and 5A). The HFC bauxite horizon belongs to the Lower Carboniferous Jiujialu formation, which has unconformable contacts with underlying Cambrian dolomite. The bauxite horizon has been divided into three sections. The lower section consists of purplish red and dark green Fe-rich clay in the lower part and the clayen pyrite aggregate in the upper. The middle section is the bauxite body, which has a dark to light gray color.

The sedimentary successions in BYT area include Precambrian Banxi Group slate and blastopsammite, Cambrian to Ordovician thick dolomite, Silurian quartz sandstone with intercalated mudstone, Devonian sandstone, shale, limestone and dolomite, Lower Permian bauxite, and Middle Permian to Cretaceous clastic rocks (Figs. 2 and 5B). Bauxite occurs in the Lower Permian Liangshan formation, overlying dolomite of the undulatory Devonian Gaopochang formation and conformably overlain by the chert and limestone of the Lower Permian Qixia formation (Fig. 2). The Liangshan formation exhibits a “coal–bauxite–iron” structure (Fig. 6A), in which the lower part consists of Fe-rich shale, the middle part consists of white to gray bauxite hosting within the sinkhole structures (Fig. 6B) and the upper part consists of coal seams, carbonaceous mudstone.

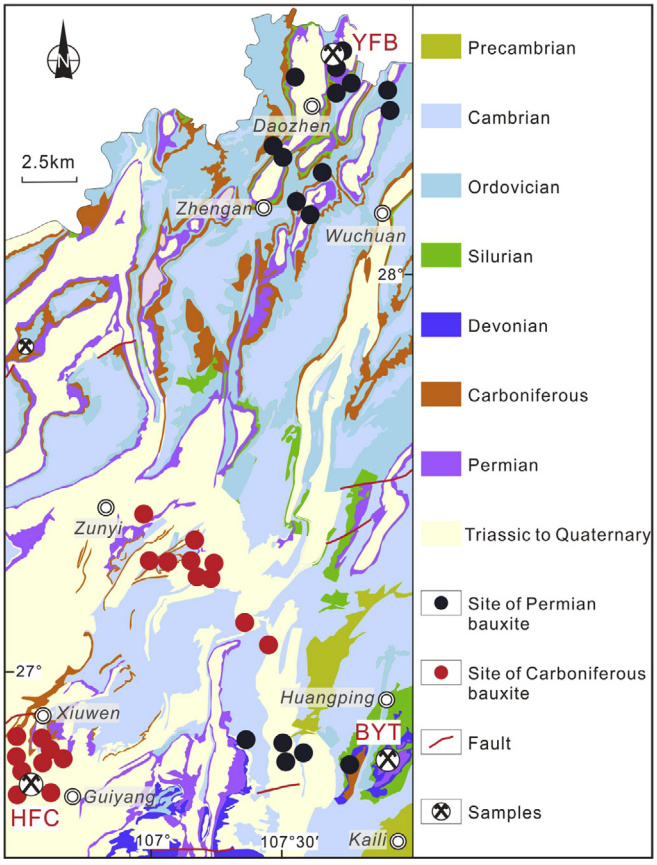

Fig. 4. Simplified geological map showing the distribution of the studied bauxite deposits.

In the YFB, the stratigraphic succession from oldest to youngest includes Cambrian, Ordovician, Silurian, Carboniferous, Permian, and Triassic lithologies. The Ordovician successions consist of dolomite, limestone and argillite. The Lower–Middle Silurian Hanjiadian formation is mainly shale, whereas the Carboniferous is dominated by limestones. The lower portion of the Lower Permian, namely Liangshan formation, correspond to the bauxitic horizon, which is overlain by the Qixia formation limestone and by argillaceous limestone. The Upper Permian contains of limestone and coal (Guizhou Bureau of Geology and Minerals, 1987). The YFB included two different substrates. One is the Silurian Hanjiadian mudstone, upon which is the pisolitic and clastic bauxite sandwiched between clay in the top and bauxitic clay in the bottom (Fig. 5C). The other is the Carboniferous limestone, upon which are the bauxitic clay and clayen pyrite in the lower, grey bauxite in the middle, and the carbonaceous mudstone and shale in the upper (Figs. 5D and 6C).

4. Analytical techniques

X-ray powder diffraction (XRPD) was conducted at the State Key Laboratory of Coal Resources and Safe Mining (China University of Mining and Technology, Beijing). XRPD analysis of powder samples was performed on a powder diffractometer (D/max-2500/PC XRPD) with Ni-filtered Cu-Kα radiation and a scintillation detector. The XRPD pattern was recorded over a 2θ interval of 2.6–60°, with a step size of 0.01°.

Detrital zircons from three bauxite samples were separated by conventional heavy liquid and magnetic techniques, then purified by hand-picking under a binocular microscope. Reflected light and cathodoluminescence (CL) images were used to identify internal structures within the zircons and to select analytical positions prior to U–Pb isotopic analyses. All the selected zircon grains were analyzed using an Agilent 7500a Laser ablation–inductively coupled plasma–mass spectrometry (LA-ICP-MS) equipped with a GeoLas200M laser source in the State Key Laboratory of Geological Processes and Mineral Resources, China University of Geosciences (Wuhan), following procedures given in Liu et al. (2007). 91500 standard was used for external standardization to correct for isotopic fractionation during analysis, with Glitter software used for off-line selection and integration of background and analytic signal, time-drift correction, and the quantitative calibration of trace element compositions and U–Pb ages. Age calculations were undertaken and concordia diagrams were constructed using Isoplot/Ex 3.00 (Ludwig, 2003), with detailed analytical procedures given in Yuan et al. (2010). The $^{206}Pb/^{238}U$ ages less than 1000 Ma were used for samples with ages > 1000 Ma, whereas $^{206}Pb/^{207}Pb$ ages were used if the initially obtained $^{206}Pb/^{238}U$ ages were > 1000 Ma (Gehrels et al., 2006; Long et al., 2010).

5. Mineralogy

In the HFC deposit, the lower part of the bauxitic sequences (sample HFC-10) is dominated by illite, clinochlore, and pyrite with small amounts of diaspore. The middle bauxitic part (samples HFC-5 and -8) is composed of diaspore with subordinateanatase and illite (Fig. 5A). The clastic bauxite ore (Fig. 7A), corresponding to the uppermost zone of the local bauxite body is overlain by an argillaceous layer (sample HFC-3), and is dominated by illite with less diaspore, boehmite, and minor anatase (Fig. 5A). The clay overlying the substrate was mainly composed of kaolinite and diaspore plus minor hematite. The bauxite ore in the middle part shows earthy and compact structure and clastic, oolitic, pisolitic texture, a white coloration (Fig. 7B) and is mainly composed of diaspore with minor anatase (Fig. 5B) The YFB, bauxite (sample YFB 01-4) developed on Silurian shale (YFB-1 profile) is compact (Fig. 7C) and composed of diaspore with some illite and clinochlore. The Silurian floor (sample YFB 01-8) is composed of clinochlore and illite (Fig. 5C). The lower part of bauxitic sequence (sample YFB 01-6) is dominated by kaolinite and illite. The upper part (sample YFB 01-2) is occurs as a clayey lithology and isdominated by illite, clinochlore and diaspore (Fig. 5C). In the sequence developed on Carboniferous limestone (YFB-2 profile, Fig. 5D), the lower parts started with gray to yellow clay (Fig. 7D) consisting of kaolinite, clinochlore, illite and boehmite (YFB 02-9). This unit is followed a pyrite-rich layer (YFB 02-10), which has only traces of diaspore (YFB 02–9). Below the bauxite a clayey bauxite unit occurs, which is dominated by kaolinite with minor boehmite (Fig. 5D). The overlying bauxite (samples YFB 02-7 and -8) is dominated by diaspore with some kaolinite and anatase.

6. Detrital zircons from bauxite

6.1. Zircon morphology

Representative CL images of the zircons, whith highlighted the analyzed spot for dating are given in Fig. 8. The size and shape of detrital zircons from the Carboniferous HFC bauxite are obviously different from those from the Permian BYT and YFB. The zircon grains of the HFC sample are 60–100 μm long with length-width ratio of 1–4. The

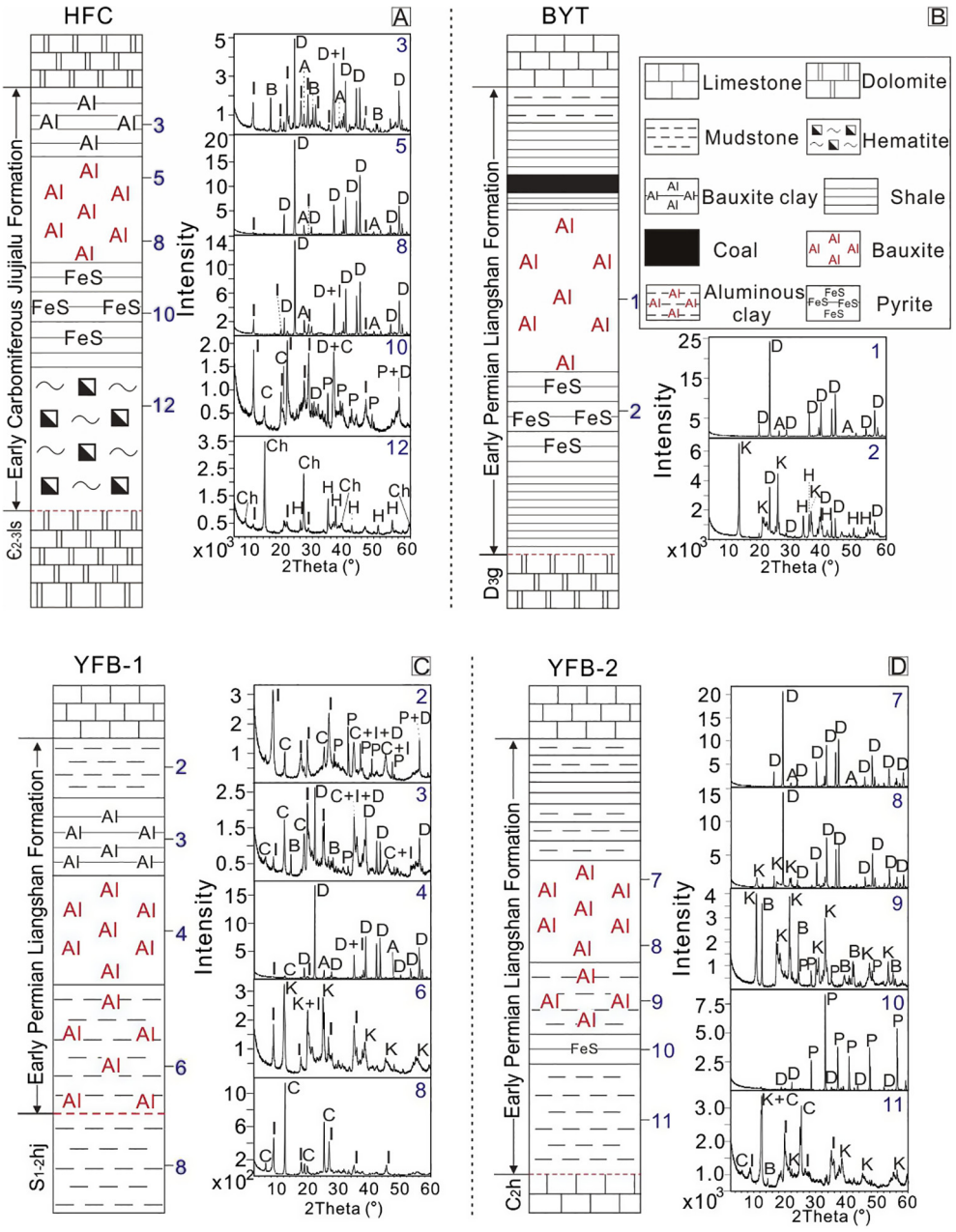

Fig. 5. Sedimentary successions and XRPD patterns of representative samples in the studied bauxite deposits. A) HFC bauxite; BYT bauxite; C) YFB-1 and D) YFB-2. Mineral abbreviations: D = diaspore; C = clinochlore; P = pyrite; H = hematite; K = kaolinite; A = anatase; I = illite; Ch = chamosite; R = rutile; B = boehmite.

zircon morphology of the HFC sample is highly heterogeneous, with shapes ranging from subhedral to euhedral, prismatic to stubby crystals, undamaged faces yet round corners. Most of the selected detrital zircon crystals show oscillatory zonation, which is indicative of an igneous origin (Hoskin and Schaltegger, 2003; Li et al., 2016); whereas others have little oscillatory zoning, suggesting a mafic igneous or metamorphic origin (Fig. 8A).

Most zircons grains collected from the YFB sample are dominated by medium sized grains with a length of 80–130 μm, and a shape ranging between subhedral to strongly rounded. A few YFB and BYT zircons have incomplete crystal faces, indicating that they have experienced a long-distance transport and an extensive abrasion (Fig. 8B). The selected detrital zircon crystals from BYT are 100–160 μm long, and subhedral to variably corroded shape. Most detrital zircon crystals selected in BYT samples show oscillatory zonation (Fig. 8C).

6.2. Detrital zircon U-Pb dating

In the 97 analyzed zircon grains from HFC bauxite, the majority yields ages between 500 Ma and 1000 Ma, with a dominant peak at ca.

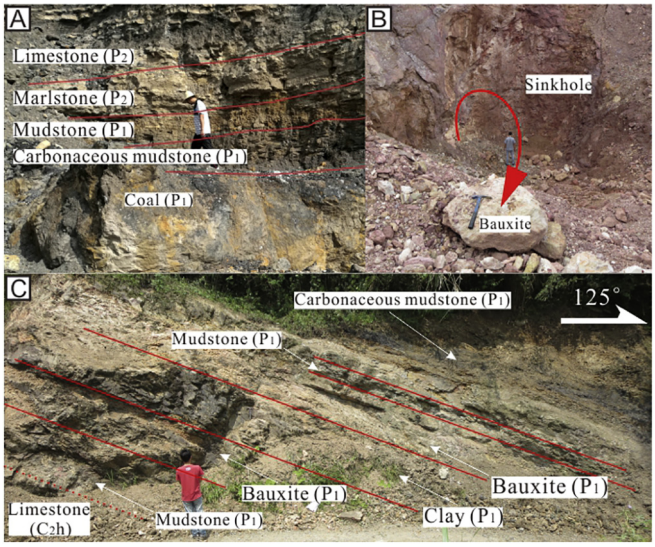

Fig. 6. Field photos illustrating the paleokarstic terrain and bauxitic sequences of the BYT and YFB bauxite deposit: (A) bauxitic sequences of BYT bauxite; P_2, Middle Permian; P_1, Early Permian; (B) sinkhole filled by bauxite in BYT; (C) bauxitic sequences of the YFB; P_1, Early Permian; C_2h, Late Carboniferous Huanglong formation.

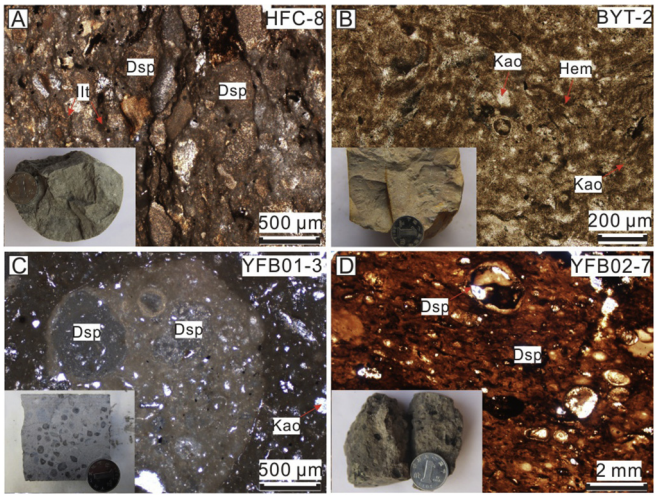

Fig. 7. Photomicrographs and hand specimen photographs of the bauxite ore in the central South China Block: (A) clastic bauxite, mineralogically composed of diaspore and some illite; (B) earthy bauxite, mainly composed of diaspore; (C) compact pelitomorphic bauxite, composed of diaspore with some illite and clinochlore; (D) diaspore-rich oöids embedded the clay matrix, polarized transmitted light.

800 Ma and minor age bumps from 500 to 540 Ma, as shown in the histogram (Fig. 9A, Supplementary Table 1). For the YFB sample, the zircon population shows age peaks at 400–600 Ma, 900–1200 Ma, 1900–1800 Ma and 2300–2600 Ma, in which the peak of 1100 Ma is the most prominent (Fig. 9B, Supplementary Table 1). The zircons for the BYT sample have ages between 500 and 2500 Ma with major peak age at 1100 Ma (Fig. 9C, Supplementary Table 1).

6.3. Zircon trace elements

Most analysed zircons have Th/U ratios ranging from 0.2 to 2 (Fig. 10A, Supplementary Table 2), suggesting a derivation from igneous rocks (Hoskin and Schaltegger, 2003; Li et al., 2016). The disparate geochemical behavior of Hf, Th, and Nb within zircon provides a discrimination criterion for judging the tectonic setting of the host (Hoskin and Schaltegger, 2003). The trace elemental compositions of the detrital zircon crystals with ages of ca. 800 Ma and ca. 1100 Ma mostly fall in the field of arc-related/orogenic in Nb/Hf versus Th/U and Hf/Th versus Hf/Nb diagrams (Fig. 10B and C, Supplementary Table 2). This is consistent with the contemporaneous ones from the regional sedimentary successions (Zhou et al., 2002; Li et al., 2003; Hofmann et al., 2015; Wang et al., 2010; Yao et al., 2011; Gu et al., 2013; Xiang et al., 2015; Yu et al., 2015).

7. Discussion

7.1. Provenance and implication for tectonic control

The Mid- to Neo-proterozoic felsic volcanic and intrusive rocks with crystallization ages of 800 Ma are widespread in the Panxi-Hannan arc along the western margin of the South China Block (Zhou et al., 2002; Li et al., 2003; Hofmann et al., 2015). Zircons with a U-Pb zircon age of ca. 800 Ma initially sourced from these felsic volcanic and intrusive rocks. Then these zircons went through many cycles of erosion and transportation and deposited in Cambrian to Devonian sedimentary rocks. Accordingly, the sedimentary units from Cambrian to Silurian commonly show a major peak at ca. 800 Ma in the detrital zircon ages. The HFC bauxite shares the similar age peak of detrital zircon with these sedimentary units (Figs. 1B and 11) (Hofmann et al., 2015; Xia et al., 2016; Wang et al., 2010). It indicates that the material of HFC bauxite came from the regional sedimentary rocks located in western South China Block.

The detrital zircon age distribution of Early Permian bauxite BYT and YFB samples show age peaks at 500–700 Ma, 900–1100 Ma, and 2400–2600 Ma (Fig. 9B and C). The major age peaks of the detrital zircons are from 900 to 1100 Ma, differing from those of the Early Carboniferous HFC bauxite. Due to the highly eroded shape of the detrital zircons, they are deduced to derive from the regional sedimentaries occurring in the center of the block, instead of the 900–1100 Ma igneous rocks sporadically distributed in the Jiangnan Orogen (Cawood et al., 2017). The age peaks of zircons from Permian bauxite BYT and YFB are comparable to the Paleozoic sediments including Cambrian, Ordovician, Silurian, and Carboniferous sediments in the center of the South China Block (Fig. 1B, Figs. 4 and 11) (Wang et al., 2010; Yao et al., 2011; Gu et al., 2013; Xiang et al., 2015; Yu et al., 2015). The Th/U ratios of 0.2–2 and the arc-related geochemical affinity of the detrital zircons in the bauxite are also compatible with those of the recycled grains in the clastic successions. Among these regional sedimentaries, the Silurian units have detrital zircons with similar age peaks to the YFB bauxite (Jing et al., 2013; Gu et al., 2013), demonstrating the more contribution to the bauxites from Silurian due to their close spatial relationship.

The intracontinental bauxite associated with marginal orogenesis, represented by those in the North China Craton, was mainly or partly derived from the volcanic rocks of the orogen (Wang et al., 2015; Cai et al., 2015). Distinct from the previous studies, this study suggests that the sedimentary units occurring within the continent are also capable to provide the source materials. It supports the previous opinion that any igneous, metamorphic or sedimentary lithology can be the parent rock

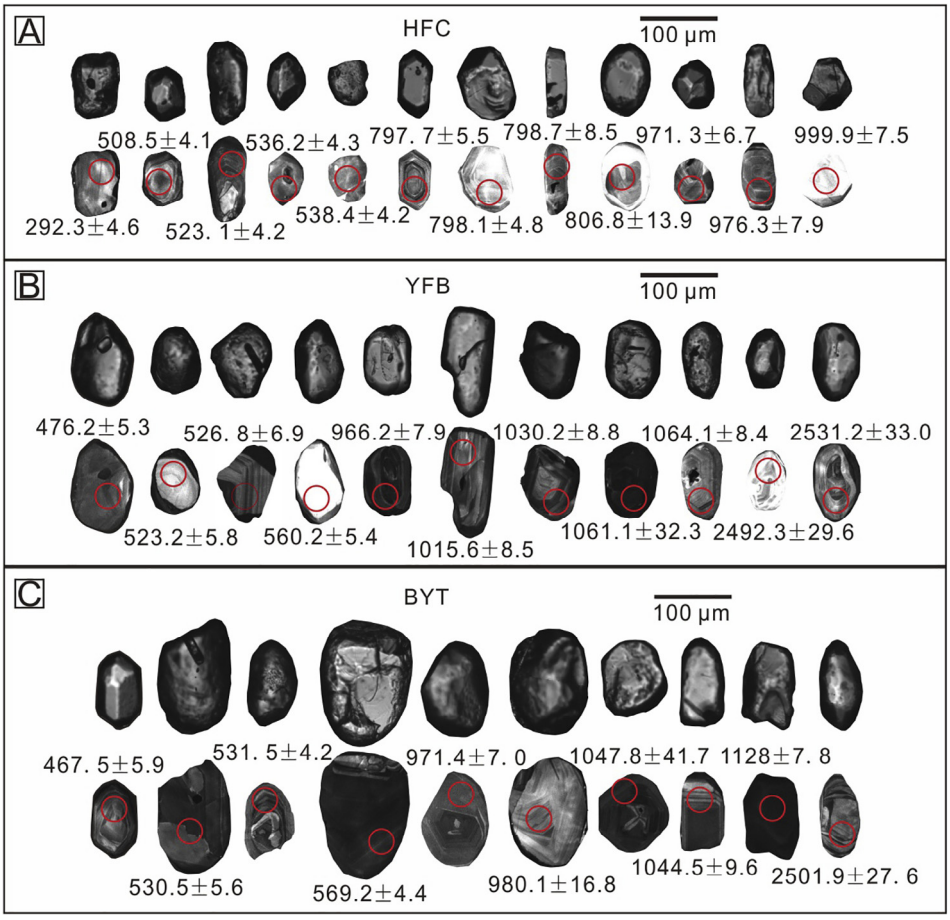

Fig. 8. Representative CL images of detrital zircon crystals from several bauxite deposits in HFC, BYT and YFB. Circles represent the analytical targets.

of bauxite under suitable conditions (D'Argenio and Mindszenty, 1995).

The changes of source region from the Early Carboniferous to Early Permian indicate a shift in the exhumation history of the study area, in particular an uplift migration from the western to the central sector of the South China Block. Tectonic studies on the subduction zones surrounding the South China Block indicate that the block has had its passive margin setting lasted from the Early Carboniferous to Permian (Li and Powell, 2001; Chen et al., 2018; Metcalfe, 2013; Wang et al., 2017) (Fig. 12). The change in provenance was probably due to the crustal extension of the passive continental margin.

7.2. Paleoclimatic and paleogeographic control

During the earlier portions of the Palaeozoic era, the surface temperatures were significantly higher accompanied by large sea-level rose. Atmospheric carbon dioxide concentrations seem to have been multiple times higher than the modern atmosphere (Fig. 2) (Berner, 1994; Berner and Kothavala, 2001). All these conditions limited the bauxitization not only by raising of groundwater table elevations but also by lowering soil moisture levels (Koster et al., 2004; Yu et al., 2018). However, the global paleoclimate changed during Early Carboniferous to Permian. The surface temperatures decreased along with the descending of in sea-level (Fig. 2) (Ross and Ross, 1988; Berner, 1990). According with the trend of the sea-level and temperature, CO_2 content in the atmosphere dropped to its lowest point (Fig. 2) (Came et al., 2007; Berner, 1991).

Lower sea-level decreased groundwater table elevations as well as exposed a large area of continental shelves for vegetation. The change of underground water level provided good drainage to leach elements from the weathering profile otherwise the weathering products tend to be low-grade bauxitic clay. The extensive vegetation facilitated bauxitization by two main factors: (1) prevent the erosion of the soft weathering products by the tropical rainstorms, (2) release a large amount of oxalic and ascorbic acids which could leach the underlying bauxitic material to improve the grade of bauxite (Kalaitzidis et al., 2010; Laskou and Economou-Eliopoulos, 2007, 2013). The bauxitization occurred in a very restricted paleogeographic zone as discussed next.

It was shown that the paleogeographic setting of the South China Block in Early Carboniferous Mississippian and Early Permian Cisuralian periods was characterized by an exposed area in the Central Yangtze Island, which was surrounded by tidal flat to restricted platform depositing clastic sediments and further off by open platform with carbonate precipitation (Ma et al., 2009; Cui, 2014). The Early

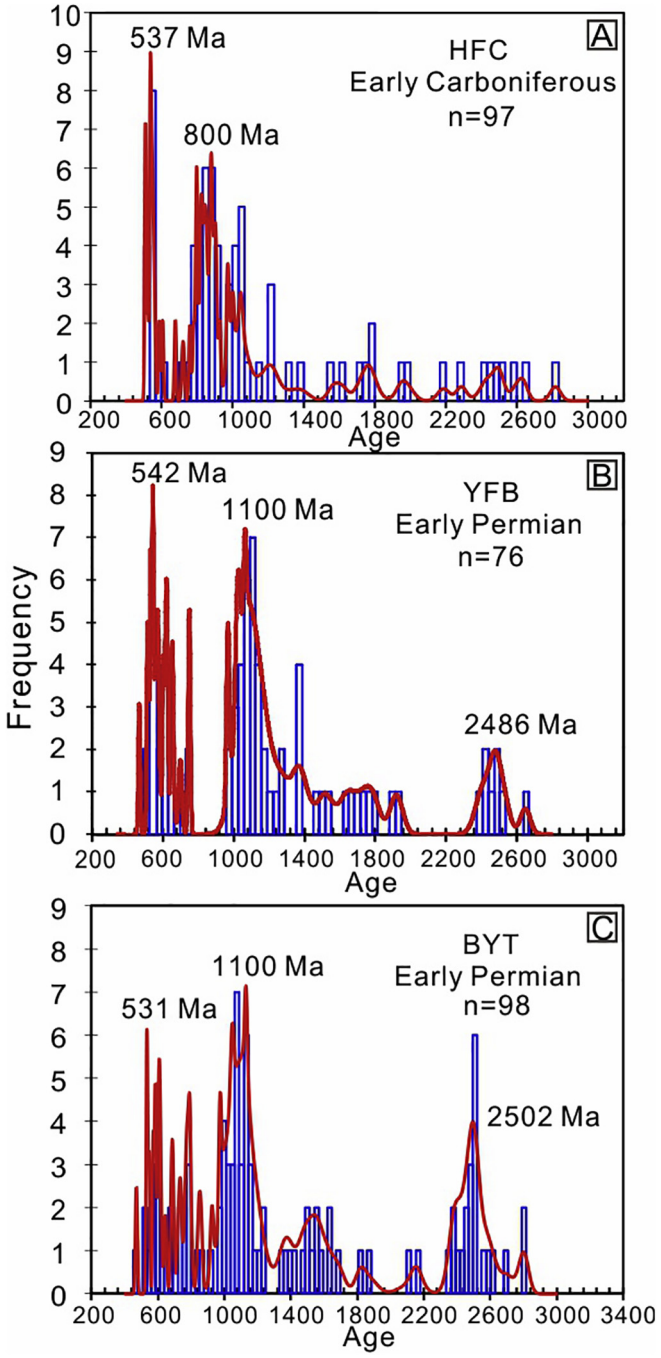

Fig. 9. Histograms of U–Pb ages of detrital zircons from HFC, YFB and BYT bauxite.

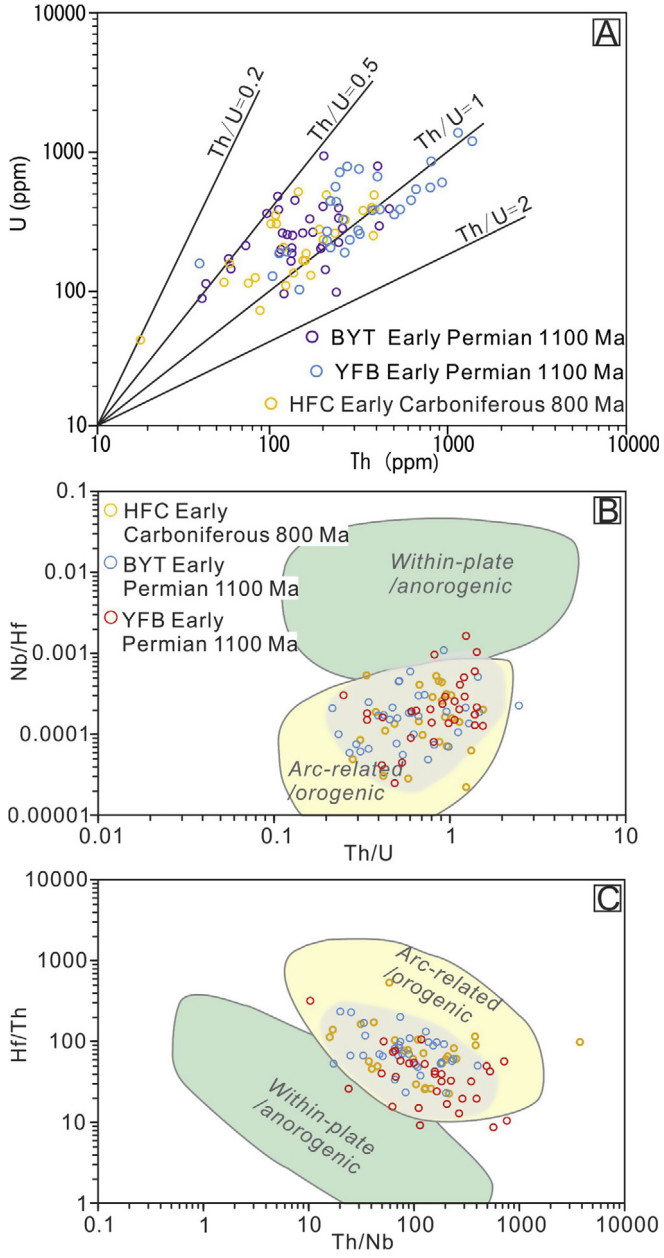

Fig. 10. (A) Th/U ratios of detrital zircon crystals from typical bauxite outcrops in the HFC, BYT and YFB horizons; (B) Th/U versus Nb/Hf and (C) Th/Nb versus Hf/Th for the ca. 800 Ma and 1100 Ma zircons. Base diagram in (B) and (C) are after Yang et al. (2012).

Carboniferous and Early Permian bauxites were situated in the tidal flat to restricted environment of the Yangtze Island (Fig. 13). Eustatic fluctuations influence the elevation of the groundwater table in these areas which promoting the formation of diaspore and leaching of silica (Özlü, 1983; Zarasvandi et al., 2008).

8. Conclusions

This study revealed combined tectonic, paleogeographic, and paleoclimatic controls on the episodic production of bauxite in an ancient island within Paleo-Tethys. In the center of the South China Block, Early Carboniferous bauxite overlying the unconformity on Upper Cambrian dolomite contains detrital zircons with a dominant age at ca. 800 Ma, which was likely recycled from the sedimentary units procured

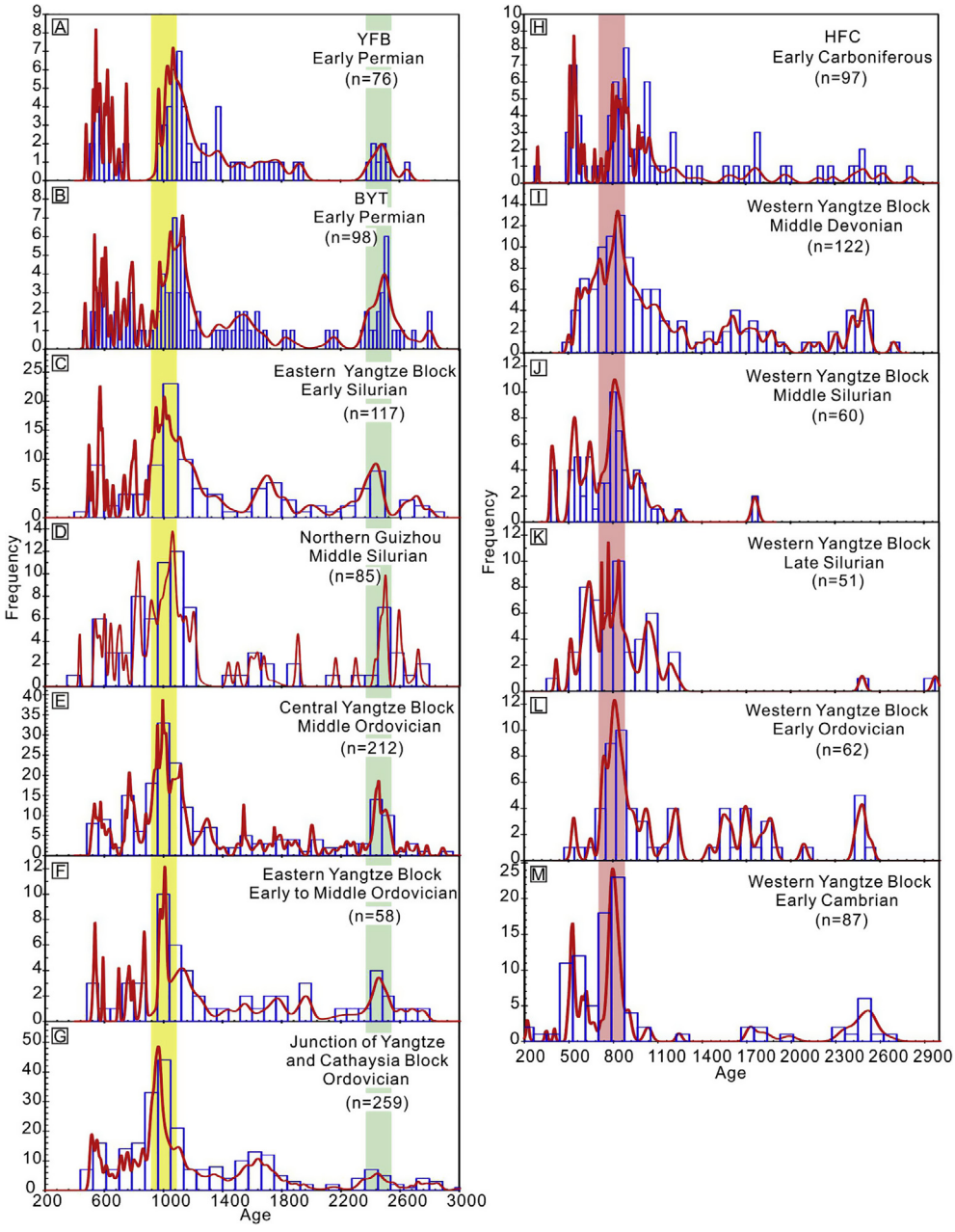

Fig. 11. Detrital zircon age distributions in Paleozoic sedimentary rocks, including: (A) the Early Permian bauxite in YFB (present study); (B) the Early Permian bauxite in BYT (present study); (C) the Early Silurian sedimentary in eastern South China Block (Yu et al., 2015); (D) the Middle Silurian sedimentary rocks in northern Guizhou (Wang et al., 2010); (E) the Middle Ordovician sedimentary successions in the central Cathaysia Block (Yao et al., 2011); (F) the Lower to Middle Ordovician sedimentary rocks in eastern South China Block (Yu et al., 2015); (G) the Ordovician sedimentary rocks at the junction of Yangtze and Cathaysia Block (Wang et al., 2015); (H) the Lower Carboniferous bauxite in HFC (the present study); (I) the Middle Devonian sedimentary in western South China Block (Xia et al., 2016); (J) the Middle Silurian sedimentary successions in western South China Block (Xia et al., 2016); (K) the Late Silurian sedimentary rocks in western South China Block (Xia et al., 2016); (L) the Lower Ordovician units in western South China Block (Xia et al., 2016); (M) the Lower Cambrian sedimentary in western South China Block (Hofmann et al., 2015). All data based on analyses with 90%-110% Concor. Concor = (($^{206}Pb/^{238}U$ age)/($^{207}Pb/^{206}Pb$)) × 100%. Ages older than 1000 Ma was calculated using $^{207}Pb/^{206}Pb$ ratios, and ages younger than 1000 Ma were calculated using $^{206}Pb/^{238}U$ ratios.

by the erosion of the 800 Ma Mid- to Neo-proterozoic felsic volcanic and intrusive rocks along the western margin of the South China Block. The Early Permian bauxite deposited unconformably upon the Upper Devonian dolomite or Silurian shale contains detrital zircons with ages ranging from 900 to 1100 Ma. These ages are consistent with that of Paleozoic sedimentary units occurring within the central sector of the South China Block. The different sources of the detrital zircons for the two bauxite horizons suggest a significant migration of the uplift from the western margin toward the central zone of the South China Block, which took place from the Early Carboniferous to the Early Permian. This migration caused the shift in provenance of the source rock of the studied bauxite deposits.

Acknowledgements

We would like to thank geological team 115, 106, and 117 for their help in fieldwork and sampling. Ramanaidou Erick is thanked for help with his constructive suggestions on this paper. This research was jointly financially supported by the National Natural Science Foundation of China (No. 41672089) and the Key Project of the Resource Exploration Bureau in Guangxi Province (No. 201649). The authors would like to thank the sponsors of China Scholarship Council (Grant No. 201706400002) for the financial support.

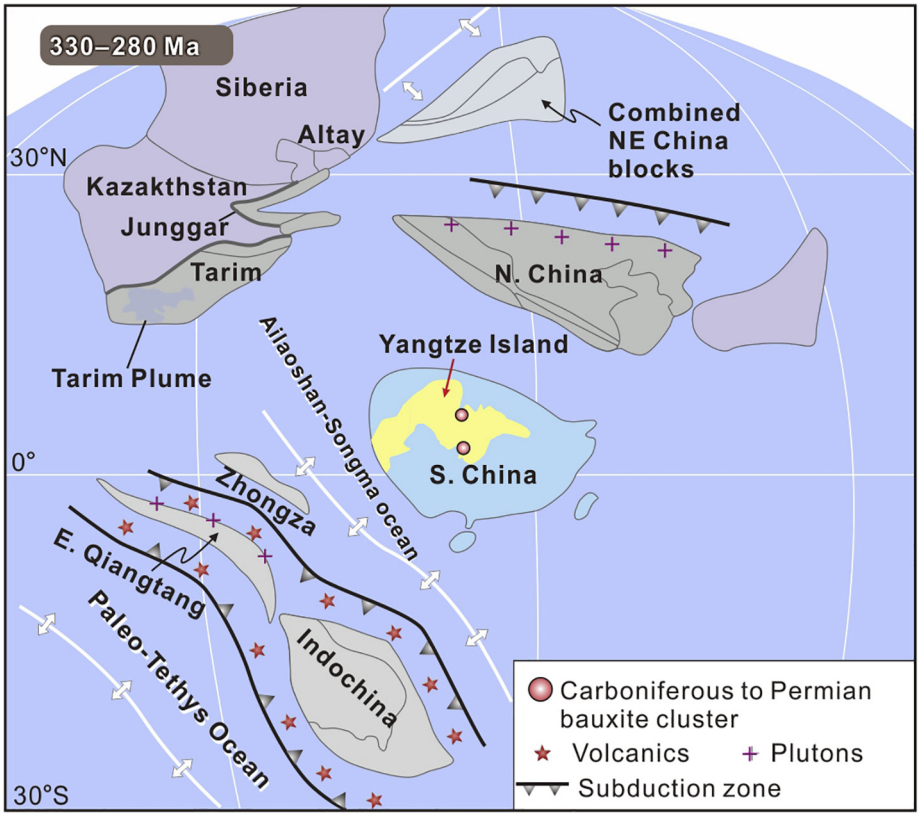

Fig. 12. Tectonic setting of the South China Block during 330–280 Ma during the bauxitization process.

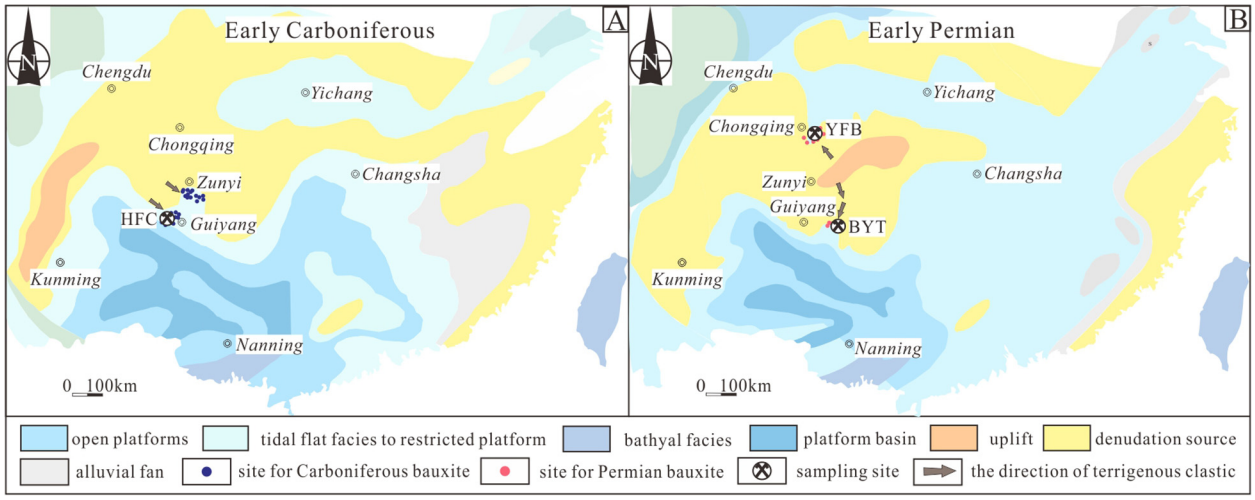

Fig. 13. Paleogeographic restoration for the bauxite genesis in the center of South China Block. (A) Early Carboniferous; (B) Early Permian.

Appendix A. Supplementary data

Supplementary data associated with this article can be found, in the online version, at https://doi.org/10.1016/j.oregeorev.2018.07.013.

References

Bárdossy, G., 1982. Karst Bauxites: Bauxite Deposits on Carbonate Rocks. Amsterdam: Elsevier Science Publishers pp. 1–441.

Berner, R.A., 1990. Atmospheric carbon dioxide levels over Phanerozoic time. Science 249 (4975), 1382–1386.

Berner, R.A., 1991. A model for atmospheric CO sub 2 over phanerozoic time. Am. J. Sci. (United States) 291 (4).

Berner, R.A., 1994. GEOCAR B II: a revised model of atmospheric CO_2 over phanerozoic time. Am. J. Sci. 294 (1).

Berner, R.A., Kothavala, Z., 2001. GEOCAR BIII: A revised model of atmospheric CO_2 over Phanerozoic time. Am. J. Sci. 301, 182–204.

Bogatyrev, B.A., Zhukov, V.V., Tsekhovsky, Y.G., 2009. Formation conditions and regularities of the distribution of large and super large bauxite deposits. Lithol. Min. Resour. 44, 135–151.

Cai, S., Wang, Q., Liu, X., Feng, Y., Zhang, Y., 2015. Petrography and detrital zircon study of late Carboniferous sequences in the southwestern North China Craton: implications for the regional tectonic evolution and bauxite genesis. J. Asian Earth Sci. 98, 421–435.

Came, R.E., Eiler, J.M., Veizer, J., Azmy, K., Brand, U., Weidman, C.R., 2007. Coupling of surface temperatures and atmospheric CO_2 concentrations during the Palaeozoic era. Nature 449 (7159), 198.

Cawood, P.A., Wang, Y.J., Xu, Y.J., Zhao, G.C., 2013. Locating South China in Rodinia and Gondwana: a fragment of greater India lithosphere? Geology 41 (8), 903–906.

Cawood, P.A., Zhao, G., Yao, J., Wang, W., Xu, Y., Wang, Y., 2017. Reconstructing South China in Phanerozoic and Precambrian supercontinents. Earth-Sci. Rev. https://doi.org/10.1016/j.earscirev.2017.06.001.

Chen, F., Wang, Q., Yang, S., Zhang, Q., Liu, X., Chen, J., Carranza, E.J.M., 2018. Space-time distribution of manganese ore deposits along the southern margin of the South China Block, in the context of Palaeo-Tethyan evolution. Int. Geol. Rev. 60 (1), 72–86.

Cocks, L.R.M., Torsvik, T.H., 2013. The dynamic evolution of the Palaeozoic geography of eastern Asia. Earth-Sci.Rev. 117, 40–79.

Cui, K., 2014. In: Regional paleogeography and evolution in Southwestern China (M). Seismological Press, pp. 119–202 (in Chinese).

D'Argenio, B., Mindszenty, A., 1995. Bauxites and related paleokarst: tectonic and climatic event markers at regional unconformities. Eclogae Geol. Helv. 88 (3), 453–499.

Deng, J., Wang, Q., Yang, S., Liu, X., Zhang, Q., Yang, L., Yang, Y., 2010. Genetic relationship between the Emeishan plume and the bauxite deposits in Western Guangxi, China: constraints from U-Pb and Lu–Hf isotopes of the detrital zircons in bauxite ores. J. Asian Earth Sci. 37, 412–424.

Deng, J., Wang, Q.F., Li, G.J., 2017. Tectonic evolution, superimposed orogeny, and composite metallogenic system in China. Gondwana Res. 50, 216–266. https://doi.org/10.1016/j.gr.2017.02.005.

Gehrels, G., Valencia, V.A., Pullen, A., 2006. Detrital zircon geochronology by Laser-Ablation Multicollector ICPMS at the Arizona Laserchron Center. Paleontological Soc. Papers 11, 67–76.

Gu, J., Huang, Z., Jin, Z., Xiang, X., 2011. Immobile Elements Geochemistry and Mass Balance Calculate of Bauxite in Wuchuan-Zheng?an-Daozhen Area, Northern Guizhou Province. China. Acta. Mineralogica. Sinica. 31 (3), 397–405.

Gu, J., Huang, Z., Fan, H., Jin, Z., Yan, Z., Zhang, J., 2013. Mineralogy, geochemistry, and genesis of lateritic bauxite deposits in the Wuchuan–Zheng'an–Daozhen area, Northern Guizhou Province, China. J. Geochem. Explor. 130, 44–59.

Guizhou Bureau of Geology and Minerals, 1987. Regional Geology of Guizhou Province. Geological Publishing House, Beijing. 555–557 (in Chinese).

Hofmann, M.H., Li, X., Chen, J., Mackenzie, L.A., Hinman, N.W., 2016. Provenance and temporal constraints of the Early Cambrian Maotianshan Shale, Yunnan Province, China. Gondwana Res. 37, 348–361.

Horbe, A.M.C., Costa, M.L.D., 1999. Geochemical evolution of a lateritic Sn–Zr–Th–Nb–Y–REE-bearing ore body derived from apogranite: the case of Pitinga, Amazonas-Brazil. J. Geochem. Explor. 66 (1–2), 339–351.

Hoskin, P.W.O., Schaltegger, U., 2003. The composition of zircon and igneous and metamorphic petrogenesis. In: Manchar, J.M., Hoskin, P.W.O. (Eds.), Zircon. Rev Mineral Geochem. 53, 27–62.

Jian, P., Liu, D., Kröner, A., Zhang, Q., Wang, Y., Sun, X., Zhang, W., 2009. Devonian to Permian plate tectonic cycle of the Paleo-Tethys Orogen in southwest China (II): insights from zircon ages of ophiolites, arc/back-arc assemblages and within-plate igneous rocks and generation of the Emeishan CF B province. Lithos 113 (3–4), 767–784.

Jing, G., Huang, Z., Fan, H., Ye, L., Jin, Z., 2013. Provenance of lateritic bauxite deposits in the Wuchuan–Zheng'an–Daozhen area, Northern Guizhou Province, China: LA-ICP-MS and SIMS U-Pb dating of detrital zircons. J. Asian Earth Sci. 70–71 (1), 265–282.

Kalaitzidis, S., Siavalas, G., Skarpelis, N., Araujo, C.V., Christanis, K., 2010. Late Cretaceous coal overlying karstic bauxite deposits in the Parnassus-Ghiona Unit, central Greece: coal characteristics and depositional environment. Int. J. Coal Geol. 81, 211–226.

Koster, R.D., Dirmeyer, P.A., Guo, Z., Bonan, G., Chan, E., Cox, P., Gordon, C.T., Kanae, S., Kowalczyk, E., Lawrence, D., Liu, P., Lu, C.-H., Malyshev, S., Mcavaney, B., Mitchell, K., Mocko, D., Oki, T., Oleson, K., Pitman, A., Sud, Y.C., Taylor, C.M., Verseghy, D., Vasic, R., Xue, Y., Yamada, T., 2004. Regions of strong coupling between soil moisture and precipitation. Science 305 (5687), 1138–1140.

Laskou, M., Economou-Eliopoulos, M., 2007. The role of microorganisms on the mineralogical and geochemical characteristics of the Parnassos-Ghiona bauxite deposits, Greece. J. Geochem. Explor. 93, 67–77.

Laskou, M., Economou-Eliopoulos, M., 2013. Bio-mineralization and potential biogeochemical processes in bauxite deposits: genetic and ore quality significance. Mineral. Petrol. 107, 471–486.

Li, G.J., Wang, Q.F., Huang, Y.H., Gao, L., Yu, L., 2016. Petrogenesis of middle Ordovician peraluminous granites in the Baoshan block: implications for the early Paleozoic tectonic evolution along East Gondwana. Lithos 245, 76–92.

Li, X., Li, W., Li, Z., Lo, C., Wang, J., Ye, M., Yang, Y., 2009. Amalgamation between the South China and Cathaysia Blocks in South China: constraints from SHRIMP U-Pb zircon ages, geochemistry and Nd–Hf isotopes of the Shuangxiwu volcanicrocks. Precambr. Res. 174 (1–2), 117–128.

Li, Z., Din, J., Xu, J., Liao, C., Yin, F., L?, T., Li, J., 2013. Discovery of the REE minerals in the Wulong-Nanchuan bauxite deposits, Chongqing, China: Insights on conditions of formation and processes. J. Geochem. Explor. 133, 88–102.

Li, Z.X., Li, X.H., Kinny, P.D., Wang, J., Zhang, S., Zhou, H., 2003. Geochronology of Neoproterozoic syn-rift magmatism in the Yangtze Craton, South China and correlations with other continents: evidence for a mantle super plume that broke up Rodinia. Precambr. Res. 122 (1–4), 85–109.

Li, Z.X., Powell, C.M., 2001. An outline of the palaeogeographic evolution of the Australasian region since the beginning of the Neoproterozoic. Earth-Sci. Rev. 53 (3–4), 237–277.

Ling, K.Y., Zhu, X.Q., Tang, H.S., Li, S.X., 2017. Importance of hydrogeological conditions during formation of the karstic bauxite deposits, Central Guizhou Province, Southwest China: a case study at Lindai deposit. Ore Geol. Rev. 82, 198–216.

Ling, K.Y., Zhu, X.Q., Tang, H.S., Wang, Z.G., Yan, H.W., Han, T., Chen, W.Y., 2015. Mineralogical characteristics of the karstic bauxite deposits in the Xiuwen ore belt, Central Guizhou Province, Southwest China. Ore Geol. Rev. 65, 84–96.

Liu, X.M., Shan, G., Di, C.R., Wu, H.L., Yuan, Hu, Z.C.,, 2007. Simultaneous in-situ determination of U-Pb age and trace elements in zircon by LA-ICP-MS in 20 ?m spot size. Chinese Sci Bull. 52 (9), 1257–1264.

Liu, X.F., Wang, Q.F., Zhang, Q.Z., Feng, Y.W., Cai, S.H., 2012. Mineralogical characteristics of the superlarge Quaternary bauxite deposits in Jingxi and Debao counties, western Guangxi, China. J. Asian Earth Sci. 52, 53–62.

Liu, K., Zhang, J., Wilde, S.A., Zhou, J., Wang, M., Ge, M., Wang, J., Ling, Y., 2017a. Initial subduction of the Paleo-Pacific Oceanic plate in NE China: Constraints from whole-rock geochemistry and zircon U-Pb and Lu–Hf isotopes of the Khanka Lake granitoids. Lithos 274, 254–270.

Liu, X.F., Wang, Q.F., Zhang, Q.Z., Yang, S.J., Liang, Y.Y., Zhang, Y., Li, Y., Guan, T., 2017b. Genesis of the Permian karstic Pingguo bauxite deposit, western Guangxi, China. Miner. Deposita 52, 1031–1048.

Long, X., Yuan, C., Sun, M., Xiao, W., Zhao, G., Wang, Y., Cai, K., Xia, X., Xie, L., 2010. Detrital zircon ages and Hf isotopes of the Early Paleozoic flysch sequence in the Chinese Altai, NW China: new constrains on depositional age, provenance and tectonic evolution. Tectonophysics. 480 (1–4), 213–231.

Long, Y., Chi, G., Liu, J., Jin, Z., Dai, T., 2017. Trace and rare earth elements constraints on the sources of the Yunfeng paleo-karstic bauxite deposit in the Xiuwen-Qingzhen area, Guizhou, China. Ore Geol. Rev. 91, 404–418.

Ludwig, K.R., 2003. User's Manual for Isoplot 3.00: A Geochronological Toolkit for Microsoft Excel. Berkeley Geochronology Center Special Publication. 1–74.

Ma, Y.S., Chen, H.D., Wang, G.L., Guo, T.L., Tian, J.C., 2009. Sequence stratigraphy and Paleogeography in south China. Beijing, China science publishing. 84-105 (in Chinese).

Metcalfe, I., 2006. Palaeozoic and Mesozoic tectonic evolution and palaeogeography of East Asian crustal fragments: the Korean Peninsula in context. Gondwana Res. 9 (1–2), 24–46.

Metcalfe, I., 2013. Gondwana dispersion and Asian accretion: tectonic and palaeogeographic evolution of eastern Tethys. J. Asian Earth Sci. 66, 1–33.

Mutakyahwa, M.K.D., Ikingura, J.R., Mruma, A.H., 2003. Geology and geochemistry of bauxite deposits in Lushoto District, Usambara Mountains, Tanzania. J. Afr Earth Sci. 36 (4), 357–369.

Nakano, N., Osanai, Y., Van, N.N., Van, T.T., 2017. Bauxite to eclogite: Evidence for late Permian supracontinental subduction at the Red River shear zone, northern Vietnam. Lithos 302–303, 37–49.

Özlü, N., 1983. Trace-element content of "Karst Bauxites" and their parent rocks in the Mediterranean belt. Miner. Deposita. 18 (3), 469–476.

Ross, C.A., Ross, J.R.P., 1988. Late Paleozoic Transgressive-Regressive Deposition. In Sea-Level Changes: An Integrated Approach. SEPM Special Publication 42.

Wang, Y., Zhang, F., Fan, W., Zhang, G., Chen, S., Cawood, P.A., Zhang, A., 2010. Tectonic setting of the South China Block in the Early Paleozoic: Resolving intracontinental and ocean closure models from detrital zircon U-Pb geochronology. Tectonics 29 (6), 1–70.

Wang, X., Jiao, Y., Du, Y., Ling, W., Wu, L., Cui, T., Weng, S., 2013. REE mobility and Ce anomaly in bauxite deposit of WZD area, Northern Guizhou, China. J. Geochem. Explor. 133, 103–117.

Wang, Q.F., Deng, J., Li, C.S., Li, G.J., Yu, L., Qiao, L., 2014. The boundary between the Simao and Yangtze blocks and their locations in Gondwana and Rodinia: constraints from detrital and inherited zircons. Gondwana Res. 26 (2), 438–448.

Wang, Q., Deng, J., Liu, X., Zhao, R., Cai, S., 2015. Provenance of Late Carboniferous bauxite deposits in the North China Craton: new constraints on marginal arc construction and accretion processes. Gondwana Res. 38, 86–98.

Wang, B., Wang, L., Chen, J., Liu, H., Yin, F., Li, X., 2017. Petrogenesis of Late Devonian-Early Carboniferous volcanic rocks in northern Tibet: new constraints on the Paleozoic tectonic evolution of the Tethyan Ocean. Gondwana Res. 41, 142–156.

Xia, X., Nie, X., Lai, C.K., Wang, Y., Long, X., Meffre, S., 2016. Where was the Ailaoshan Ocean and when did it open: A perspective based on detrital zircon U-Pb age and Hf isotope evidence. Gondwana Res. 36, 488–502.

Xiang, X.L., Jin, Z.G., Huang, Z.L., Zhou, J., Jing, G.U., 2015. Origin of Ore-forming Materials for Bauxite Deposits in Northern Guizhou Province, China: evidence from Detrial Zircon U-Pb Dating. Acta Miner. Sin.

Yang, L., 2018. Proto-to Paleo-Tethyan evolution of the eastern margin of Simao block. Gondwana Res. https://doi.org/10.1016/j.gr.2018.02.012.

Yang, J., Cawood, P.A., Du, Y., Huang, H., Huang, H., Tao, P., 2012. Large Igneous Province and magmatic arc sourced Permian-Triassic volcanogenic sediments in China. Sed. Geol. 261–262, 120–131.

Yang, L., Wang, Q., Zhang, Q., Carranza, E.J.M., Liu, H., Liu, X., Deng, J., 2017. Interaction between karst terrain and bauxites: evidence from Quaternary orebody distribution in Guangxi, SW China. Sci. Rep. 7 (1), 11842.

Yang, S.J., Wang, Q.F., Zhang, Q.Z., Chen, J.H., Huang, Y.X., 2018. Terrestrial deposition processes of quaternary gibbsite nodules in the Yongjiang Basin, southeastern margin of Tibet, and implication for the genesis of ancient karst bauxite. Sediment Geol. https://doi.org/10.1016/j.sedgeo.2018.06.010.

Yao, J., Shu, L., Santosh, M., 2011. Detrital zircon U-Pb geochronology, Hf-isotopes and Geochemistry-New clues for the Precambrian crustal evolution of Cathaysia Block, South China. Gondwana Res. 20 (2–3), 553–567.

Yu, W., Du, Y., Cawood, P.A., Xu, Y., Yang, J., 2015. Detrital zircon evidence for the reactivation of an Early Paleozoic syn-orogenic basin along the North Gondwana margin in South China. Gondwana Res. 28 (2), 769–780.
Yu, W., Thomas, J.A., Yan, J., Yang, J., Du, Y., Huang, X., Weng, S., 2018. Climatic and hydrologic controls on upper Paleozoic bauxite deposits in South China. Earth-Sci. Rev. https://doi.org/10.1016/j.earscirev.2018.06.014.
Yuan, H., Gao, S., Liu, X., Li, H., Günther, D., Wu, F., 2010. Accurate U-Pb Age and Trace Element Determinations of Zircon by Laser ablation-inductively coupled plasma-mass spectrometry. Geostandards Geoanalyt. Res. 28 (3), 353–370.
Zarasvandi, A., Charchi, A., Carranza, E.J.M., Alizadeh, B., 2008. Karst bauxite deposits in the Zagros mountain belt, Iran. Ore Geol. Rev. 34 (4), 521–532.
Zhao, G., 2015. Jiangnan Orogen in South China: developing from divergent double subduction. Gondwana Res. 27 (3), 1173–1180.
Zhao, G., Cawood, P.A., 2012. Precambrian geology of China. Precambr. Res. 222, 13–54.
Zhao, J.H., Zhou, M.F., Yan, D.P., Zheng, J.P., Li, J.W., 2011. Reappraisal of the ages of Neoproterozoic strata in South China: no connection with the Grenvillian orogeny. Geology 39 (4), 299–302.
Zhou, M.F., Yan, D.P., Kennedy, A.K., Li, Y.Q., Ding, J., 2002. SHRIMP U-Pb zircon geochronological and geochemical evidence for Neoproterozoic arc-magmatism along the western margin of the Yangtze Block, South China. Earth Planet Sci. Lett. 196 (1–2), 51–67.